Physics of Fluids

RESEARCH ARTICLE | JUNE 20 2023

Understanding the yielding behavior of graphene oxide colloids via experimental strain decomposition

Shim Yul Hui (심율희) ; Simon A. Rogers

Physics of Fluids 35, 063117 (2023)
https://doi.org/10.1063/5.0156022

Physics of Fluids ARTICLE pubs.aip.org/aip/pof

Understanding the yielding behavior of graphene oxide colloids via experimental strain decomposition

Cite as: Phys. Fluids **35**, 063117 (2023); doi: 10.1063/5.0156022
Submitted: 25 April 2023 · Accepted: 3 June 2023 ·
Published Online: 20 June 2023

View Online Export Citation CrossMark

Yul Hui Shim (심율희), and Simon A. Rogers[a)]

AFFILIATIONS

Department of Chemical and Biomolecular Engineering, University of Illinois at Urbana-Champaign, Urbana, Illinois 61801, USA

[a)]Author to whom correspondence should be addressed: sarogers@illinois.edu

ABSTRACT

Graphene oxide (GO) has attracted attention in materials science and engineering due to its large aspect ratio and dispersibility in polar solvent including water. It has recently been applied to direct-ink-writing (DIW) printing to realize the fabrication of three-dimensional structures, suggesting a wide variety of potential applications. Without post-processing, DIW printing requires yield stress fluids to fully build three-dimensional objects. The key properties of these inks are the yield stress and the viscoelastic properties during yielding. DIW ink rheology has therefore received significant interest in materials science, as well as mechanical and chemical engineering. Despite this interest, the yielding process has not been clearly elucidated and understanding yielding remains an outstanding problem. In this study, we discuss the yielding behavior of GO colloids via oscillatory rheology by decomposing the total strain into the recoverable and unrecoverable parts through iterative experimental techniques. The recoverable and unrecoverable responses represent viscoelastic solid and plastic properties, respectively, and they are used to determine the averaged storage and dissipation of energies. By mapping these contributions, we more clearly elucidate the yielding behavior of the GO colloids and suggest guidelines for energy efficiency. Beyond the specific lessons learned regarding the DIW-relevant rheology of GO colloids, our study contributes to an evolving development of material-centric and energy-focused methods for understanding the out-of-equilibrium rheological physics associated with the yielding of soft materials.

I. INTRODUCTION

Graphene oxide (GO) has been widely exploited in materials science and engineering due to its ability to form large-area alignments and a wide range of rheological properties,[1–4] which are controlled with lateral size,[5,6] concentration,[7,8] and adding polymer or salt.[9–11] The excellent dispersibility and ease of controlling the rheological properties allow GO to be prepared as a colloidal system, and GO colloids can be used in various processes involving shear force such as bar/blade coating,[12–14] spinning,[15–18] and 3D printing.[9,19–21] Among these processes, direct-ink-writing (DIW) printing has recently attracted attention to realize the fabrication of complex three-dimensional (3D) structures from the GO colloids, suggesting potential applications in soft robotics, batteries, or sensors. In DIW printing with yield stress fluids (YSFs), the key properties are the yield stress and the post-yielding viscosity that lead to the rheological transitions called yielding and unyielding. During yielding, the material behavior changes from that of a viscoelastic solid to that of a fluid. Unyielding is the reverse process. During the printing process, DIW inks experience both yielding, as the ink is extruded, and unyielding as the stresses drop below the yield stress once a filament has left the nozzle.[22–24] The yielding transition is typically thought of as being dependent on the applied shear force and is a direct result of the inherent colloidal interactions and allows the material to be extruded as a fluid,[25,26] but to then resolidify to support weight.[27,28]

Ink rheology has been highlighted in materials science, mechanical, and chemical engineering.[22–33] Many studies on nonlinear rheology of soft materials in general and DIW printing with GO or graphene-based inks, in particular, have established routine shearing protocols. Flow curves, in which the steady-state stress or viscosity is plotted against the shear rate, are commonly collected to determine the yield stress, which is related to the ability to support the weight of the 3D structure. Flow curves are also used to confirm that YSF inks exhibit shear-thinning behavior, which is often said to be required when the ink is extruded from the nozzle. A simple argument shows this line of reasoning to be flawed, because any YSF will be shear thinning simply by the presence of the yield stress. Take, for example, the

case of the simple inelastic Bingham model, for which the flow stress is the sum of a yield stress and a flow rule:

$$\sigma_{\text{Bingham}} = \sigma_y + \eta_B \dot{\gamma},$$

where σ_y is the yield stress, η_B is the Bingham viscosity, and $\dot{\gamma}$ is the shear rate. The viscosity is the ratio of the stress to the shear rate, which for the Bingham model is

$$\eta_{\text{Bingham}} = \frac{\sigma_{\text{Bingham}}}{\dot{\gamma}} = \frac{\sigma_y}{\dot{\gamma}} + \eta_B.$$

At low rates, the Bingham viscosity is dominated by the $\sigma_y/\dot{\gamma}$ term, which enforces shear thinning with a slope of the viscosity vs shear rate curve of −1. The presence of the yield stress therefore enforces shear thinning.

Another protocol in common use to distinguish viscoelastic properties is oscillatory shear testing. Oscillatory rheology is most commonly characterized by the storage (G′) and loss (G″) moduli. The storage modulus in the linear regime, G'_{LVR}, is typically frequency independent in YSF and is believed to represent the ability to retain the shape of the extruded ink and its architecture. The value of G'_{LVR} is often compared across various ink systems.[9]

Despite ink rheology being emphasized and shear protocols being established, there is still a lack of clear understanding regarding how inks yield. Effective guidelines for process conditions are therefore also missing, and trial-and-error is still used to find shear conditions when printing with new materials or different compositions. Additionally, an incomplete understanding of yielding and unyielding leads to critical issues, such as unexpected manufacturing of low-quality products and waste of materials and energy. Avoiding these problems requires a fundamental understanding of rheological transitions.

To understand yielding behavior, oscillatory shear testing ranging from small to large amplitudes allows us to interpret the rheological properties at a given flow strength and timescale.[34–36] The amplitude sweep results are usually interpreted by comparing the magnitude of G′ and G″, which are traditionally interpreted as the elastic and viscous properties, respectively. For example, YSFs typically show a larger G′ than G″ at small amplitudes, while G″ becomes larger than G′ as the amplitude increases. The point where G′ and G″ intersect has been referred to as the flow point and is one of many definitions in use to describe yielding conditions.[21,37–40] Oscillatory shear testing is also often used as a tool to relate the stiffness or yield point of the materials by comparing G'_{LVR} and the flow point, but these measures still lack clear understanding regarding their physical meanings. It can be said that our inability to clearly define accurate yielding measures reflects our incomplete understanding of how materials yield.

A recently introduced experimental technique, recovery rheology, was used to show that G″ is a composite parameter, consisting of components relating to the dissipation of energy from recoverable and unrecoverable processes.[41–44] This indicates that the common interpretation of G′ and G″ as elastic and viscous properties, respectively, is an oversimplification, and that the yielding behavior of materials is more nuanced and must be understood in terms of the measurable energetic terms.

The key concept of recovery rheology is the experimental decomposition of strain into recoverable and unrecoverable strains. The idea of recoverable and unrecoverable strains originated with the studies of Weissenberg[45] and Reiner.[46] The two components can be determined during any protocol by adding a zero-stress step immediately after the deformation of the material. The recoverable strain (γ_{rec}) is the amount of strain that recovers when the stress is removed, while the unrecoverable strain (γ_{un}) is the amount that remains without fully returning to its initial state. The recoverable and unrecoverable components can be interpreted as the contributions from the viscoelastic solid and plastic properties, respectively.

Within the recovery rheology framework, the dynamic moduli are clearly interpreted only in terms of energetic contributions and can be used to describe the large amplitude oscillatory shear (LAOS) behavior of the material by decomposing G″ into two parameters obtained from recoverable (viscoelastic solid) and unrecoverable (plastic) components. Donley *et al.* elucidated in 2020 that the G″ overshoot, a typical behavior of YSFs, is due to a continuous transition from recoverable to unrecoverable acquisition of strain from small to large amplitudes.[42] From the decomposition of recoverable and unrecoverable components, the Kamani–Donley–Rogers (KDR) model was proposed in 2021.[43] The KDR model can accurately predict the rheology of simple yield stress fluids, demonstrating that yielding is a continuous behavior. In the following year, Griebler *et al.* studied nonlinear rheology of yield stress foods using both recovery rheology experimental techniques and also the KDR model.[44]

In this study, we elucidate how the GO colloids yield during oscillatory shear testing via experimental strain decomposition and suggest effective process guidelines for the extrusion during DIW printing. We present the amplitude sweep results for GO colloids using recovery rheology and provide a deep understanding of material deformations from small amplitude oscillatory shear (SAOS) to LAOS. We also compare the rheological transitions of two types of GO colloid, noting that the yielding and LAOS behaviors are strongly dependent on the microstructure and interaction of GO sheets. The details to prepare two types of GO colloids, a suspension and a gel, are discussed in Sec. II A. Both GO colloids exhibit almost identical G′ and G″ in the LVR but different G″ trends as shown in Sec. III A: GO suspension and gel are classified as LAOS type I and type III,[47] respectively. As shown in Fig. 1, the difference between types I and III is the presence or absence of overshoot in G″. In Sec. III B, their rheological transitions are examined through the decomposed moduli. In Sec. III C, we investigate the contribution from the viscoelastic solid component from SAOS to LAOS and suggest a method of describing the energy efficiency for the process. Our method is general and can be applied to a wide range of

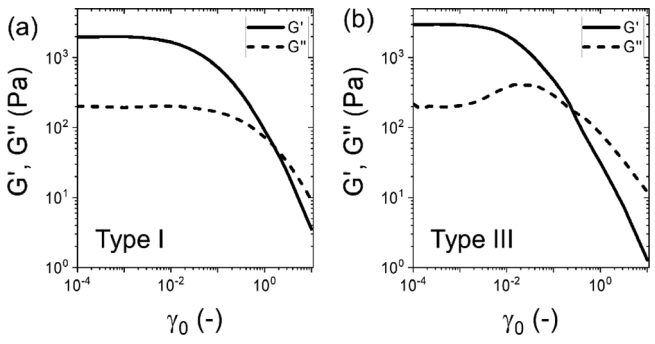

FIG. 1. Typical strain amplitude sweeps, with type designations from Hyun *et al.* (a) Type I (strain thinning) and (b) type III (weak strain overshoot).

materials. In Sec. III D, we analyze the yielding of GO colloids by comparing the viscoelastic solid and plastic deformations and also propose an energetic Deborah number to describe the material deformation.

II. MATERIAL AND EXPERIMENTAL METHODS

A. Graphene oxide colloids

Graphene oxide (GO) suspension was supplied from STANDARD GRAPHENE. The concentration of the GO stock suspension dispersed in de-ionized water is 1 wt %. The GO has a lateral dimension of 8 μm with an approximate thickness of 1 nm. To prepare the high-concentration of GO suspension (4.7 wt %), the desired amount of water was removed using a centrifuge (15 000 rpm, 6 h). The salt stock solution was prepared by pouring calcium dichloride ($CaCl_2$) at 5 wt % into de-ionized water and mixing for 2 min using a vortex.

A sample diluted only with de-ionized water in the high-concentration of GO stock suspension is referred to as the "GO suspension." In contrast, a sample prepared by adding the salt solution to a GO stock suspension is referred to as the "GO gel." The divalent cation (Ca^{2+}) in this study acts as a cross-linker to form hydrogel through a coordination interaction with oxygenated functional groups of GO sheet in the supplementary material (Fig. S1).[9,48–50] All samples were mixed with a Thinky mixer running at 2000 rpm for 30 min. We performed amplitude sweep tests of GO suspension and gel samples of various compositions in the supplementary material (Fig. S2). Among them, the representative samples exhibiting almost identical G′ and G″ were selected to demonstrate that yielding behavior cannot be explained by the linear VE properties solely. The representative samples used in this study are the GO suspension at a concentration of 4.2 wt % GO and the GO gel at a concentration of 0.86 wt % GO and 0.12 wt % salt.

B. Rheometry

Rheological measurements were performed on an MCR-302 rheometer from Anton Paar using a 2° cone-plate geometry with a 50 mm diameter at 25 C. In some cases, additional evaporation protection was provided by humidifying the air in the evaporation blocker via a water bubbler. The frequency sweep tests before and after each main measurement were compared to confirm that there was no critical issue in solvent evaporation. To distinguish between experimental paradigms, we refer to "traditional rheology" as being characterizations based on total strains and rates, while "recovery rheology" characterizes behavior in terms of recoverable and unrecoverable strains and rates. The traditional characterization in Fig. 3 was performed using standard functions inside the RheoCompass software.

C. Iterative recovery tests for recovery rheology

The recovery rheology experiments were performed by using the list function inside the steady strain measurement option in RheoCompass. Each data point of oscillation is imported to the software with a resolution of 512 points per period and frequencies of 1 rad/s. Each recovery test begins with four full periods of oscillation to allow for the steady alternating state to be reached, followed by a partial period of oscillation and then immediately by a zero-stress recovery step lasting 42 s. The ultimate recoverable strain is obtained by subtracting the strain value at the end of the recovery interval from the total strain right before the application of zero stress. A graphical description of this process is shown in Fig. 2. The partial period of oscillation changes where the zero-stress step begins, depending on where the period is being examined. The recovery points were located at intervals of every 8 points out of a total of 512 points per period, resulting in a resolution of 64 points per period.

Through iterative recovery tests, the total strain is decomposed into the recoverable and unrecoverable strains, and their numerical derivatives are the strain rates of each component. Strains and strain rates are used to calculate moduli and viscosities. The decomposed strain can be used to define more informative descriptions of the dynamic moduli that reflect the storage of energy and the rate of energy dissipation.[42,51] The storage and loss moduli that are used traditionally can be calculated based on the total strain and strain rate as follows:

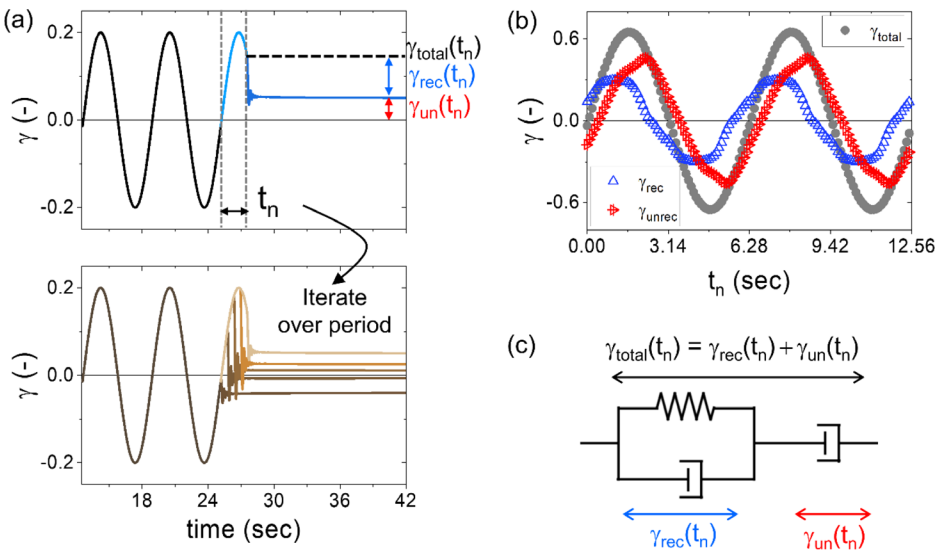

FIG. 2. (a) Graphical description of recovery tests. (b) The decomposed strain through iterative recovery tests resulting in a resolution of 64 points per period. (c) Jeffreys model that supports recovery rheology.

$$G'(\omega) = \frac{4[W_s(\omega)]_{avg}}{{\gamma_0}^2} = \frac{2[\gamma(t)\sigma(t)]_{avg}}{{\gamma_0}^2}, \quad (1)$$

$$G''(\omega) = \frac{2\left[\dot{W}_d(\omega)\right]_{avg}}{\omega{\gamma_0}^2} = \frac{2[\dot{\gamma}(t)\sigma(t)]_{avg}}{\omega{\gamma_0}^2}. \quad (2)$$

Using recovery rheology, the dynamic moduli are also decomposed into recoverable and unrecoverable portions. The work of Donley *et al.* defined *three* dynamic moduli, including *two* loss moduli, using decomposed strains as follows:

$$G'_{solid}(\omega) = \frac{4\left[W_{s,solid}(\omega)\right]_{avg}}{{\gamma_0}^2} = \frac{2[\gamma_{rec}(t)\sigma(t)]_{avg}}{{\gamma_0}^2}, \quad (3)$$

$$G''_{solid}(\omega) = \frac{2\left[\dot{W}_{d,solid}(\omega)\right]_{avg}}{\omega{\gamma_0}^2} = \frac{2[\dot{\gamma}_{rec}(t)\sigma(t)]_{avg}}{\omega{\gamma_0}^2}, \quad (4)$$

$$G''_{fluid}(\omega) = \frac{2\left[\dot{W}_{d,fluid}(\omega)\right]_{avg}}{\omega{\gamma_0}^2} = \frac{2[\dot{\gamma}_{unrec}(t)\sigma(t)]_{avg}}{\omega{\gamma_0}^2}. \quad (5)$$

The subscripts "solid" and "fluid" relate to recoverable and unrecoverable strains, respectively. These decomposed dynamic moduli show that there is one storage modulus, and that it is associated with the acquisition of recoverable strain G'_{solid}, while the loss modulus is a composite parameter that can be recast as the sum of two terms that are associated with the rates at which strain is acquired recoverably and unrecoverably, G''_{solid} and G''_{fluid}.

Consideration of the Jeffreys model is helpful to understand the concepts of recovery rheology. The Jeffreys model consists of a spring and dashpot connected in parallel and a dashpot connected separately in series, where the parallel/series parts represent the recoverable/unrecoverable components, as shown in Fig. 2(c). In the Jeffreys model, the spring is related to the recoverable storage of energy, while the dashpots connected in parallel or series are related to the recoverable or unrecoverable rates of energy dissipation, which in turn lead to retardation and relaxation effects.[52] Thus, the recoverable component can represent the viscoelastic solid properties, while the unrecoverable component can represent the plastic properties.

III. RESULTS AND DISCUSSION

A. Traditional rheological characterization

Traditional rheological characterizations include a measurement of the steady-shear flow curve, frequency sweeps, and amplitude sweeps to observe the dynamic moduli from SAOS to LAOS. We show in Fig. 3(a) the flow curves of both the GO suspension and gel. They are well described by the Herchel–Bulkley model with dynamic yield stresses close to 80 and 40 Pa, respectively. That the yield stress of the suspension is higher than that of the gel means that the GO suspension slumps less and is able to support more mass before slumping, as shown in the inset of Fig. 3(a). Since both samples are yield stress fluids, in the linear regime their dynamic moduli are almost independent of the frequency, with the storage modulus being much larger than the loss modulus, as shown in Fig. 3(b).

The amplitude sweep results are shown in Fig. 3(c). The moduli of both GO suspension and gel are similar at small and large amplitudes, but they show different behaviors at intermediate amplitudes. In traditional amplitude sweep tests, only the gel sample exhibits significant overshoot in the loss modulus. The two GO colloids can be classified according to the scheme of Hyun and coworkers[47] into different LAOS types depending on the presence or absence of the overshoot in the loss modulus: the GO suspension is categorized as type-I (no overshoots in dynamic moduli), while the GO gel is categorized as type-III (overshoot in G'' only).

B. Recoverable and unrecoverable moduli

The decomposed moduli, obtained from recoverable and unrecoverable strains, are presented in Fig. 4. As shown in Fig. 4(a), the moduli associated with viscoelastic solid behavior, G'_{solid} and G''_{solid}, of the GO suspension remain constant at small amplitudes but start to decrease as the amplitude increases. The modulus associate with unrecoverable acquisition of strain, G''_{fluid}, exhibits an overshoot with a gradual increase up to around a strain amplitude of 0.65 and then decreases at larger amplitudes. The GO suspension, which does not present an overshoot in the traditional loss modulus, G''_{trad}, was classified as a type-I material. Despite this categorization on the basis of the total strain response, it has a clear overshoot in G''_{fluid}, which is masked by the balance of G''_{solid} and G''_{fluid}.

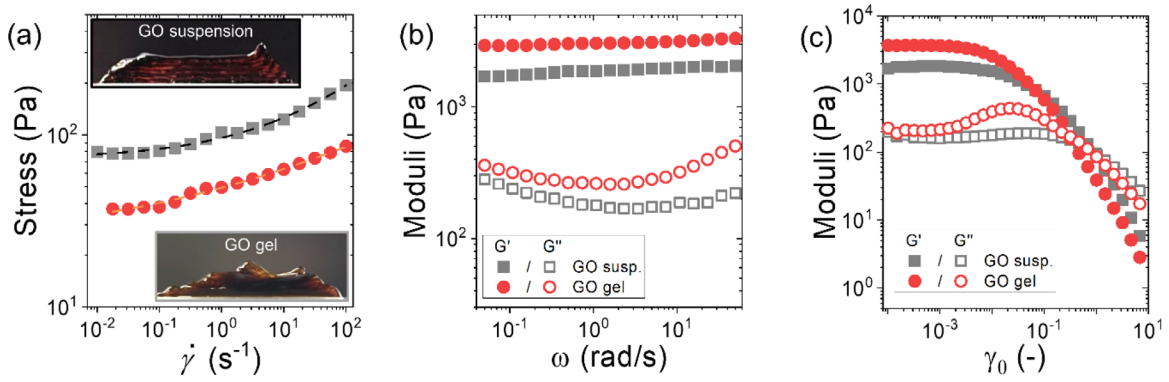

FIG. 3. Traditional rheological characterization for GO suspension (gray symbol) and gel (red symbol). (a) Steady-shear flow curves with the Herschel–Bulkley fit are shown in dashed lines. The insets show the stacked ink for two GO colloids. (b) Linear regime frequency sweeps at a strain amplitude of 0.1%. (c) Traditional amplitude sweep results for GO suspension and gel at a frequency of 1 rad/s.

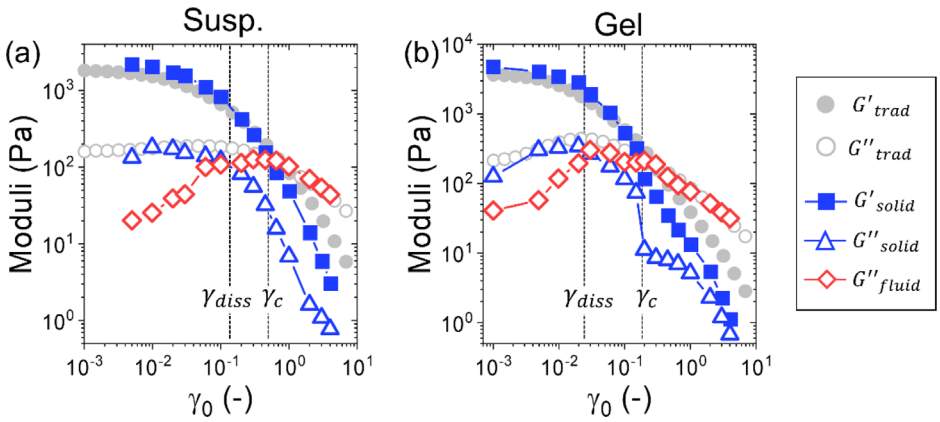

FIG. 4. Decomposed amplitude sweeps for (a) GO suspension and (b) gel at 1 rad/s.

In contrast, the gel that was classified as a type-III material because of the overshoot in G''_{trad} exhibits overshoots in *both* the decomposed moduli shown in Fig. 4(b). The G''_{trad} overshoot of the gel comes at smaller amplitudes from the influence of G''_{solid} followed by the larger amplitude influence of G''_{fluid}. Both sets of observations are consistent with the study of Donley *et al.* that revealed that the yielding is a continuous transition from viscoelastic (VE) solid to plastic contribution.[42]

Since the traditional loss modulus is a composite parameter that can be decomposed into VE solid and plastic acquisitions, it suggests that LAOS type-I and type-III can be further subdivided according to the decomposed moduli, G''_{solid} and G''_{fluid} [details are in the supplementary material (Fig. S3)].

The recovery rheology moduli allow us to qualitatively compare the yielding behavior of the two GO colloids, which display noticeable differences, especially at intermediate amplitudes. The GO gel shows a previously unreported overshoot in G''_{solid} in addition to the broad overshoot in G''_{fluid} observed by Donley *et al.* for a variety of yield stress fluids. The different yielding behaviors can be attributed to the microstructural differences of the two GO colloids. The GO gel, which has a network structure[9,48–50] because the GO sheets are crosslinked by Ca^{2+}, can compress and extend its network structure like a sponge before fully yielding. At large amplitudes, the GO gel finally behaves like a fluid and can flow, indicating that the network structure has broken, perhaps into small agglomerates. These behaviors collectively contribute to the overshoot in G''_{solid} at intermediate amplitudes and the sudden drop of G''_{solid} at large amplitudes. In the GO suspension, the GO sheets are densely dispersed without chemical bonding and form an ordered nematic liquid crystal structure due to the negative charge on the surface of the GO sheet.[3,8,11] Thus, at large amplitudes, the yielding behavior can result from the rearrangement of GO sheets along the shear direction,[14,16,53–55] exhibiting gradually decreased G''_{solid}.

Although the two GO colloids have different yielding behaviors, they share some common phenomenology because both GO colloids are yield stress fluids. Both GO colloids show overshoots in G''_{fluid}, implying an increased contribution of the plastic component to dissipated energy. This behavior, rather than an overshoot in G''_{trad}, can be interpreted as being typical of yielding.

As the amplitude increases, G''_{fluid} passes through two intersections. One is the intersection of the two loss moduli (G''_{fluid} and G''_{solid}), γ_{diss}, which is located around strain amplitudes of 0.1 and 0.02 in the suspension and gel. The other intersection is where G'_{solid} and G''_{fluid} meet, γ_c, which, because of the magnitude of G''_{solid} at large amplitudes, is equivalent to the traditional G'-G'' crossover point. This crossover of moduli has been referred to as the flow point.[21,37–40] In the suspension and the gel, the flow point lies near strain amplitudes of 0.6 and 0.15.

The G''_{fluid}-G''_{solid} intersection indicates the point where the dominant contribution of the dissipated energy of the material response passes from the VE solid to the plastic, while the G'_{solid}-G''_{fluid} intersection represents the point at which the energy stored elastically begins to become less than the energy dissipated plastically divided by the angular frequency [see Eqs. (3) and (5)]. Both intersections of the gel are found at lower amplitudes than those of the suspension, implying that the gel yields at small perturbations compared to the suspension. The details will be discussed in Sec. III D and Fig. 5.

The amplitude sweeps can be divided into three regimes based on γ_{diss} and γ_c: (i) small, (ii) intermediate, and (iii) large amplitudes. Each regime has noticeable features for the GO suspension and gel as follows:

(i) When $\gamma_0 < \gamma_{diss}$, $G'_{solid} > G''_{solid} > G''_{fluid}$.
(ii) When $\gamma_{diss} < \gamma_0 < \gamma_c$, $G'_{solid} > G''_{fluid} > G''_{solid}$.
(iii) And when $\gamma_0 > \gamma_c$, $G''_{fluid} > G'_{solid} > G''_{solid}$.

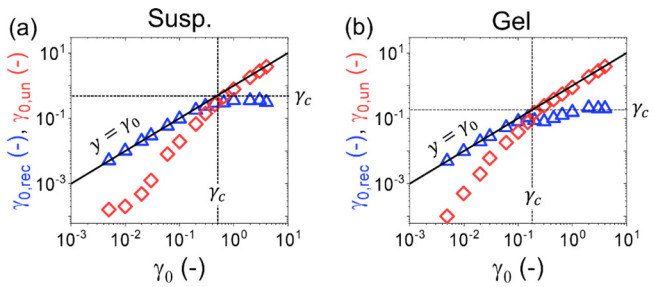

FIG. 5. Decomposed strain amplitude for (a) the GO suspension and (b) gel. The black solid line represents the total strain amplitude as a function of y = x. The horizontal and vertical dashed lines indicate the amplitude value at the flow point (G′ and G″ crossover points in Fig. 4).

It is noteworthy that there is no amplitude at which any of the moduli are zero or even unmeasurably small over all amplitudes we have explored. Rather, there are always measurable quantities of recoverable and unrecoverable strains even at the smallest amplitudes we probed. This supports the idea that yielding is not a digital behavior, as is assumed in the Oldroyd–Prager formalism, but is rather a continuous transition.[56,57]

C. Stored energy from VE solids in LAOS

To compare the contributions from the VE solid and plastic deformation, we show in Fig. 5 the recoverable and unrecoverable strain amplitudes as a function of the total strain amplitude (γ_0). At small amplitudes, almost all of the strain is recoverable and $\gamma_{0,rec} \approx \gamma_0$. As the total amplitude increases, the recoverable and unrecoverable strains gradually increase until the flow point (γ_c), when the recoverable and unrecoverable amplitudes become equal, $\gamma_{0,rec} = \gamma_{0,un}$, and the recoverable strain amplitude saturates. The recoverable strain amplitude does not exceed beyond γ_c, implying that γ_c is the maximum value of the recoverable strain at a given frequency. That is, recovery rheology presents a clear physical interpretation of the strain amplitude at which the dynamic moduli cross, γ_c: it is the maximum amount of recoverable strain acquired by the system.

The saturated recoverable strain amplitude indicates that the stored energy from VE solid is always present even when the material "flows" at large amplitudes and that even at further high shear forces, its value levels off. However, as shown in Fig. 4, G'_{solid} does not level off and continues to decrease as the amplitude increases. The moduli G'_{solid}, G''_{solid}, and G''_{fluid} are normalized by the total strain amplitude and are therefore suitable for comparing against the traditional moduli, which are normalized in a similar way as shown in Eqs. (1)–(5). However, given that recovery rheology takes the perspective that strain is separable, it is more effective to normalize the component moduli by their respective component strain amplitudes, such as

$$G'_{solid,raw} = \frac{4W_{s,solid}}{\gamma_{0,rec}{}^2} = \frac{2\left[\sigma(t)\gamma_{rec}(t)\right]_{avg}}{\gamma_{0,rec}{}^2}. \quad (6)$$

To investigate the contribution of VE solid response at the material scale during yielding, we plot in Fig. 6 $G'_{solid,raw}$ and compare it with G'_{solid}, reflecting the difference from total and recoverable strain amplitudes. The amplitude sweep results are divided into the same three regimes as used in Fig. 4. Both GO colloids show similar trends for each regime: (i) $G'_{solid,\ raw}$ is equivalent to G'_{solid} because the contribution in VE solid deformation accounts for most of the total material response at small amplitudes; (ii) at intermediate amplitude, the decreasing slope of G'_{solid} is slightly steeper than that of the $G'_{solid,\ raw}$. As the contribution from plastic deformation becomes prominent, the total amplitude is no longer accounted for by the recoverable deformation only, and acquisition of unrecoverable strain begins to dominate; and (iii) at large amplitudes above the point at which $G' = G''$, the recoverable strain amplitude remains constant, and thus $G'_{solid,raw}$ levels off. This result is consistent with the discussion of Fig. 5.

The data of Figs. 6(c) and 6(d), which show the elastic Lissajous curves in which the stress is plotted parametrically vs the total strain, allow for a simple way to get $G'_{solid,raw}$ without the iterative recovery rheology tests. While $G'_{solid,raw}$ represents the average energy stored

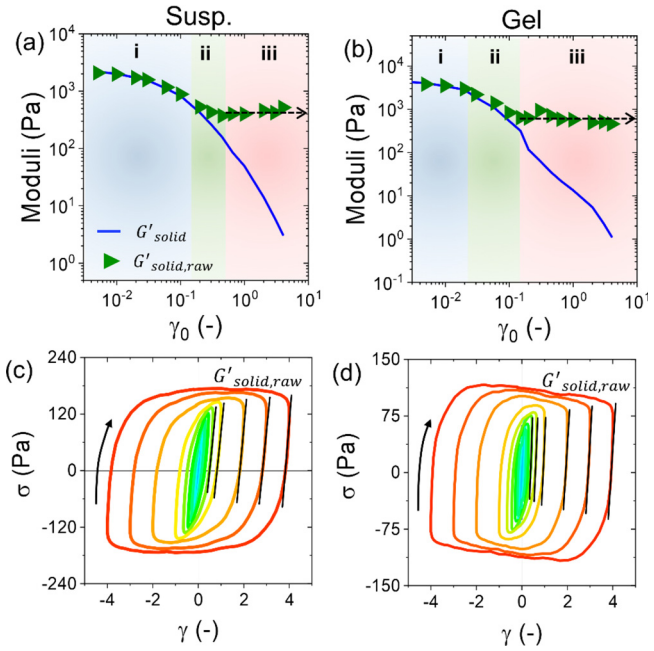

FIG. 6. The G'_{solid} and $G'_{solid,raw}$ for (a) GO suspension and (b) gel. The three regimes marked with different colors are divided based on the intersections, γ_{idss} and γ_c. Elastic Lissajous curves for (c) GO suspension and (d) gel. The slope of the lines represents the $G'_{solid,raw}$ equal to the apparent cage modulus, $G_{cage} = \partial\sigma/\partial\gamma|_{\sigma=0}$.

elastically normalized by the recoverable strain amplitude, the elastic Lissajous curve allows us to interpret the instantaneous modulus at a given frequency and amplitude. $G'_{solid,raw}$ is equal to the instantaneous slope of the elastic Lissajous curve at zero stress, as indicated by the black solid lines in Figs. 6(c) and 6(d). The instantaneous slope at zero stress was defined as the apparent cage modulus, $G_{cage} = \partial\sigma/\partial\gamma|_{\sigma=0}$, by Rogers in 2011.[58] In highly concentrated colloidal systems, the mobility of colloids is hindered by their nearest neighbors that form an effective cage. When the colloidal system is sheared, the cage is deformed, showing linear elastic properties, and at larger strains, the cage eventually breaks, causing yielding and flow. The apparent cage modulus represents the cage elasticity as follows:

$$G'_{solid,raw} = d\sigma/d\gamma|_{\sigma=0} = G_{cage}. \quad (7)$$

Therefore, the elastic properties at the material scale ($G'_{solid,\ raw}$) can be equated to the cage elasticity, which can be obtained as an instantaneous slope of the elastic Lissajous curve at zero stress without iterative recovery rheology tests.

The equivalence between $G'_{solid,raw}$ and G_{cage} allows us to confirm that the VE solid contribution is always present, even in the LAOS regime. The saturation of $G'_{solid,raw}$ indicates that there is an upper limit to the amount of energy storable elastically, as shown in the supplementary material (Fig. S4). In this case, therefore, imposing high shear forces and larger total strains does not result in more deformation at the scale responsible for recover, e.g., polymer chain conformation, agglomerates breaking, or particle alignment, implying that more processing energy may be wasted.

D. Dissipated energy competition: VE solid vs plastic deformation

The dissipated energy can be decomposed into contributions from VE solid and plastic deformations acquired from recoverable and unrecoverable strain rates, respectively. Therefore, the material's behavior can be interpreted as the stress responses from the three components, as shown in Fig. 7.

The decomposed strain allows us to create three new Lissajous curves by plotting the stress against the recoverable strain [Figs. 7(a) and 7(d)], recoverable rate [Figs. 7(b) and 7(e)], and unrecoverable rate [Figs. 7(c) and 7(f)], which can be interpreted as energy stored in VE solid, energy dissipated in VE solid, and energy dissipated in plastic deformation, respectively.

The GO suspension and gel have different magnitudes of the recoverable strain/rate and the unrecoverable rate at a given amplitude, but they have the same trends where the three components gradually increase as the amplitude increases. The recoverable elastic Lissajous curves in Figs. 7(a) and 7(d) show the ellipsoid, which have a linear slope corresponding to the $G'_{solid,\ raw}$. As the amplitude increases, the ellipsoid expands symmetrically around the slope ($G'_{solid,\ raw}$), but there is a limit to the expansion along the recoverable strain axis, as indicated by the dashed line. This is consistent with the discussion of Fig. 5.

As the amplitude increases, the recoverable viscous Lissajous curves [Figs. 7(b) and 7(e)] distort, while the unrecoverable viscous Lissajous curves [Figs. 7(c) and 7(f)] gradually decrease in slope. In Figs. 7(c) and 7(f), the dotted line indicates the slope, which is equivalent to the viscosity ($\eta_{flow} = 2[\sigma(t)\dot{\gamma}_{un}(t)]_{avg}/(\dot{\gamma}_{0,un})^2 \cong G''_{unrec}/\omega$). The decreasing slope in both GO colloids indicates shear-thinning behavior. Further details can be found in the supplementary material (Fig. S6).

The recoverable strain reaches a limit at a certain point, but the recoverable/unrecoverable rates continue to increase, expanding their viscous Lissajous curves in two dimensions. This suggests that the VE solid (recoverable) and plastic (unrecoverable) deformation are in competition as the amplitude increases, and their results affect yielding and flowing. Therefore, interpreting the response of a material with a clear distinction between recoverable and unrecoverable components can lead to a deeper understanding of the yielding behavior.

We show in Fig. 8 the recoverable and unrecoverable viscous Lissajous curves divided into the same three regions as in Fig. 4. The stress varies with component rates during the oscillation cycle, indicating that the stress is influenced by the different amounts that each component rate acquires instantaneously.

At small amplitudes (Fig. 8-i), the stress is maximum when the unrecoverable rate is zero, implying that the flow viscosity is close to infinity and plastic deformation is negligible instantaneously. In contrast, at intermediate amplitudes (Fig. 8-ii), the unrecoverable rate at maximum stress moves away from zero, indicating that plastic deformation is getting predominant as the strain increases. While the recoverable rate is predominant below γ_c (at small and intermediate amplitudes), in Fig. 8-iii, the unrecoverable rate is larger than the recoverable rate above γ_c (at large amplitudes), suggesting that plastic deformation is dominant.

The traditional and new Lissajous curves are plotted as the stress vs strain or rate, so the material's behavior is interpreted by focusing on the stress response. Considering that all components share a common stress response, the 3D curves consisting of two rate components and stress are created in Figs. 9(a) and 9(b). A new projection of 3D curve is displayed in Fig. 9(b) composed of recoverable and unrecoverable rates; the component rate Lissajous curve was introduced by Kamani and Donley *et al.*[49]

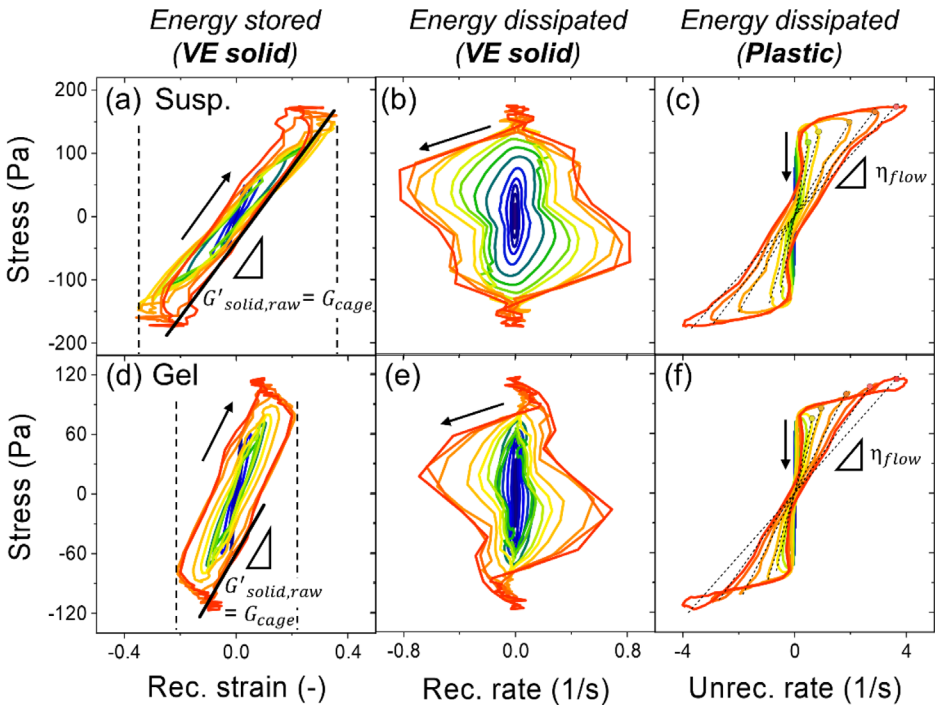

FIG. 7. New Lissajous curves containing decomposed strain and strain rate for (a)–(c) GO suspension and (d)–(e) gel: stress vs [(a) and (d)] recoverable strain, [(b) and (e)] recoverable rate, and [(c) and (f)] unrecoverable rate. The traditional Lissajous curves containing total strain and total rate are in the supplementary material (Fig. S5).

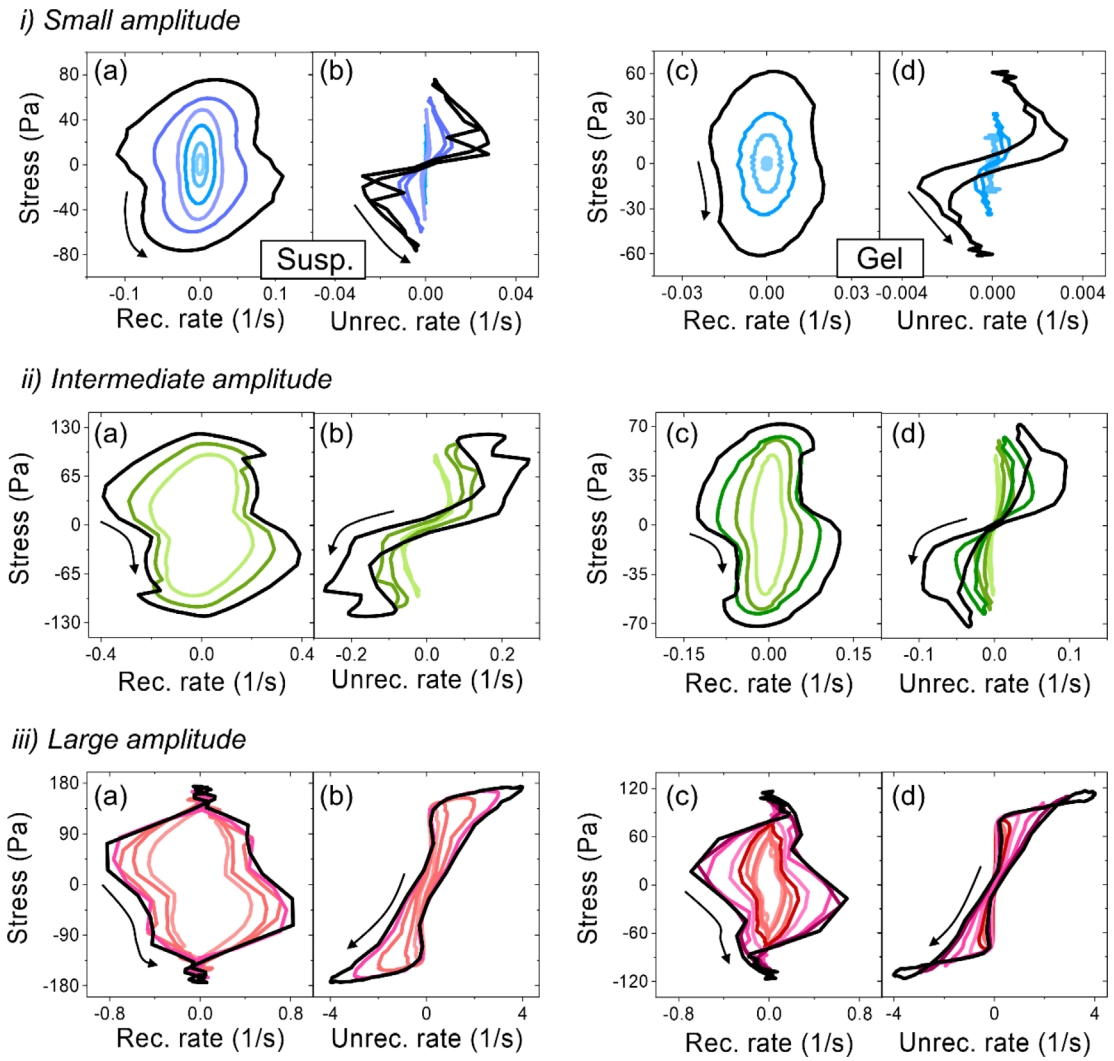

FIG. 8. Lissajous curves plotting by the stress against [(a) and (c)] recoverable rate and [(b) and (d)] unrecoverable rates for [(a) and (c)] GO suspension and [(b) and (d)] gel. The three regimes, (i)–(iii), are divided based on the intersections, γ_{idss} and γ_c: (i) small amplitude, $\gamma_0 < \gamma_{idss}$; (ii) intermediate amplitude, $\gamma_{idss} < \gamma_0 < \gamma_c$; and (iii) large amplitude, $\gamma_c < \gamma_0$.

The component rate Lissajous curves provide a clear way for us to understand the transient yielding behavior by comparing the contributions from VE solid and plastic responses. The shaded area where the recoverable rate is greater than the unrecoverable rate is interpreted as exhibiting solid-like deformation, while the white area is interpreted as fluid-like deformation.

The component rate Lissajous curves for the GO suspension and gel at each regime are shown in Fig. 10. All curves of both GO colloids at small amplitude (Fig. 10-i) span the solid-like deformation indicated as a shaded regime. As the strain increases, the curves in Fig. 10-ii pass to the fluid-like deformation regime, while most of the curves in Fig. 10-iii are in the fluid-like deformation regime. Plastic flow is easily identified as being the region where the unrecoverable rate steeply changes and the recoverable rate is close to zero, as indicated by the red arrow in Fig. 10-iii. The presentation of the component rate curves provides further support that yielding occurs through a continuous transition from solid-like to fluid-like deformation.

The component rate Lissajous curves allow us to interpret and compare the transient yielding behavior for the GO suspension and gel. Both GO colloids exhibit more solid-like deformation predominantly at small amplitudes and more fluid-like deformation at large amplitudes. Their different microstructures are reflected at intermediate amplitudes, where distinct trajectories of the component rate Lissajous curve are exhibited.

When reading the trajectories shown in Fig. 10, gradual yielding is observed when the material response moves from the recoverable rate to the unrecoverable rate axis,[59] while gradual unyielding is interpreted when the response moves from the unrecoverable rate to the recoverable rate axis. The yielding and unyielding are repeated within the oscillation cycle.

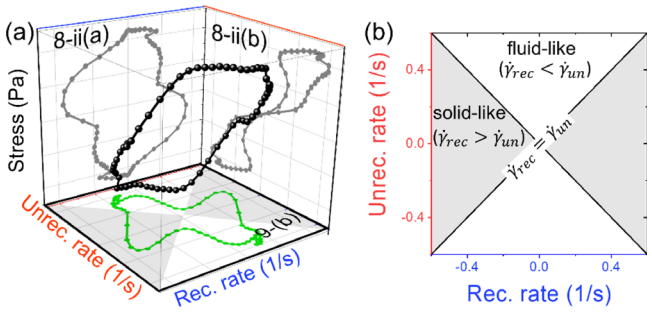

FIG. 9. (a) 3D Lissajous curve showing relationships in stress and unrecoverable/recoverable rates. The curve represents the result for GO suspension at a strain of 45%. (b) The new component rate Lissajous curve plotting by two decomposed strain rates. On the basis of the diagonal solid lines, the material response is divided into solid-like and fluid-like regimes, shown in gray and white triangles, respectively.

The GO gel response, marked as the green arrow in Fig. 10(b-ii), shows that the recoverable rate reduces but the unrecoverable rate remains almost constant. This implies that the instantaneous yielding and unyielding simultaneously occur at intermediate amplitude. The crosslinker Ca^{2+} in the GO gel allows it to form a network structure composed of GO agglomerates, which can be broken at high shear forces. As long as the strain is insufficient to completely break the network structure, the agglomerates can be partially broken and also reformed at the same time, exhibiting the local yielding behavior.

At large amplitudes, the network structure of the GO gel can be broken down from large to small agglomerates, and finally, plastic flow is possible as indicated by the red arrow in Fig. 10-iii, whereas the GO suspension without chemical bonds allows plastic flow as the GO sheets are gradually reoriented along the shear direction.[14,16,53–55]

In Fig. 11, all curves, representing large, intermediate, and small amplitudes, show the same slope in the shaded area as indicated by the black solid line. This implies that the transient yielding can initiate

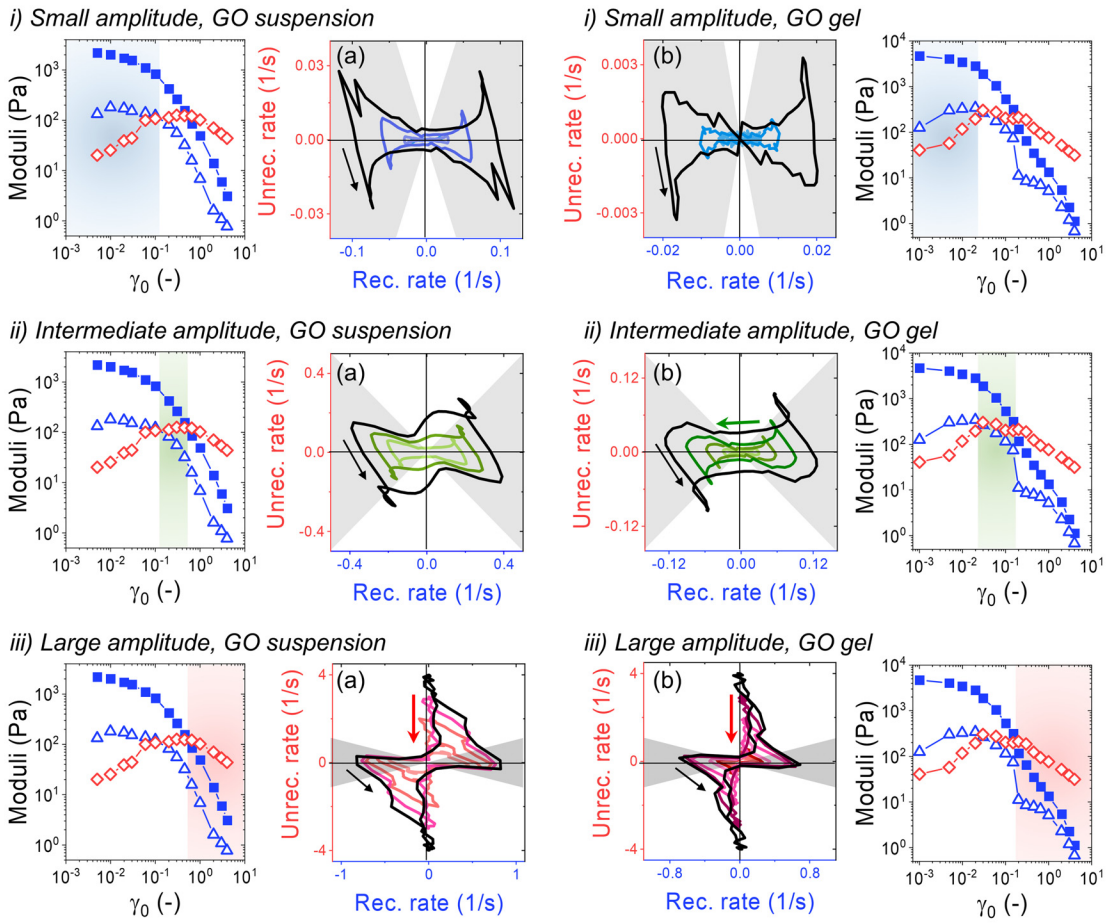

FIG. 10. The component rate Lissajous curve for (a) GO suspension and (b) gel. The shaded regimes in the component rate Lissajous curve represent that the deformation is instantaneously more solid-like. The black arrow indicates the direction of the trajectory. The graphs at both ends are the same amplitude sweep graphs as in Fig. 4, with each amplitude regime indicated by different colors.

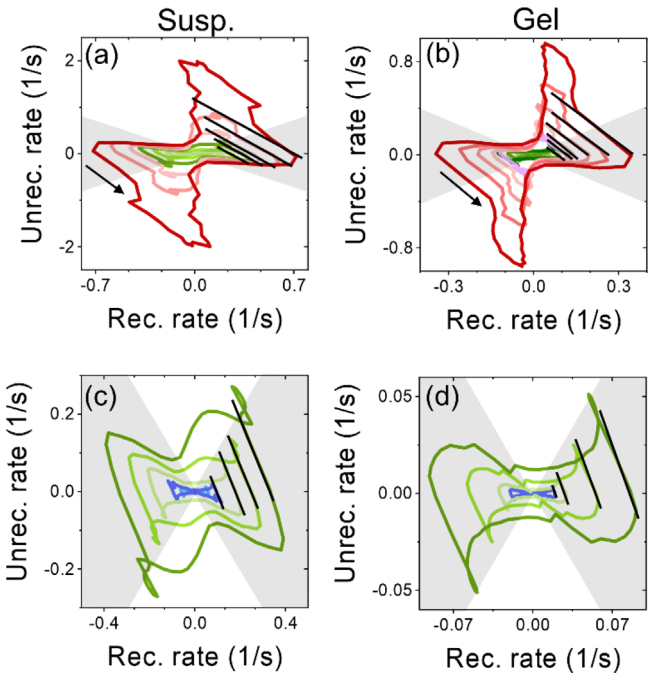

FIG. 11. The component rate Lissajous curve [(a) and (b)] at large and intermediate amplitudes and [(c) and (d)] at intermediate and small amplitudes. The black solid lines indicate the slope in the shaded area. The slope is the same at all amplitudes. The black arrow indicates the direction of trajectory.

even at small amplitudes, though it is not allowed to go to completion by the restricted application of strain. Therefore, in an oscillatory shearing test, the materials can always exhibit some features of transient yielding behavior regardless of the magnitude of the amplitude.

The observation that yielding initiates at small amplitudes but is not allowed to progress to completion indicates that the common interpretation of binary yielding, that a material either flows or not, can be misleading. Rather, a quantitative description of how slowly or quickly the material flows is required. Furthermore, considering that materials' yielding is a continuous transition, it is necessary to quantify the material deformation into solid-like or fluid-like behaviors under shear forces at a given timescale.

The Deborah number, De, is defined as the ratio of the material's relaxation time to the experimental observation time.[60,61] The Deborah number is used to describe how solid-like or liquid-like a material response may be. If the Deborah number is greater/less than 1, it is interpreted that the material exhibits solid-/fluid-like behaviors.

In oscillatory tests, the experimental observation time in Reiner's definition of the Deborah number is typically taken to be the inverse of the frequency, so that $\mathrm{De} = \lambda\omega$, where λ is the relaxation time and ω is the angular frequency. However, the relaxation time of any yield stress fluid, including GO colloids, is too long to measure with a rheometer. Additionally, although the relaxation time of a material can be measured, it is typically determined in the linear viscoelastic regime, so the traditional definition of De should be avoided in amplitude sweeps where the material response exhibits nonlinear behavior and changes from being elastically dominated at small amplitudes and to viscously dominated at larger amplitudes for yield stress fluids. Using the traditional definition applied to oscillatory tests, both the small and large amplitude behaviors would be assigned the same Deborah number, even though the physics of the two extremes is clearly different.

To avoid these issues, attempts to redefine the Deborah number have been proposed using recovery rheology, particularly focusing on the transient behavior. In 2021, Singh *et al.* suggested a new dimensionless number that meets Reiner's goals for defining the Deborah number.[62] Reiner's original suggestion was that the Deborah number should (1) be defined as the ratio of two timescales and (2) be able to describe the relative extent of elastic and viscous effects expected in the behavior of solids and fluids. Thus, Singh *et al.* (re)defined the Deborah number as the ratio of recoverable and unrecoverable strain rates in an instantaneous manner as follows:

$$De_t(t) = \frac{\dot{\gamma}_{rec}(t)}{\dot{\gamma}_{unrec}(t)}. \tag{8}$$

This proposed definition can represent the instantaneous material behaviors for steady-shear startup and creep tests, but it leads to a variation during oscillatory shearing from 0 to ∞ twice per period.

Solving this limitation, Kamani *et al.* developed an instantaneous definition of the Deborah number that describes the materials' response to oscillatory shearing as follows:[59]

$$De_t(t) = \sqrt{\frac{\dot{\gamma}_{rec}(t)\ddot{\gamma}_{rec}(t)}{\dot{\gamma}_{unrec}(t)\ddot{\gamma}_{unrec}(t)}}. \tag{9}$$

Their study contributed to understanding the intracycle nonlinear behavior by showing the transient Pipkin space described in terms of instantaneous dimensionless groups.

Here, we propose a dimensionless number that provides similar information to the Deborah number and is based on the rates at which energy is dissipated in recoverable and unrecoverable processes as follows:

$$E_{solid/fluid} = \frac{\dot{W}_{d,solid}}{\dot{W}_{d,fluid}} = \frac{\left[\sigma(t)\dot{\gamma}_{rec}(t)\right]_{avg}}{\left[\sigma(t)\dot{\gamma}_{un}(t)\right]_{avg}}. \tag{10}$$

Each dissipated energy is proportional to the area of one of the recovery rheology Lissajous curves as shown in Fig. 12. At a given frequency and amplitude, two dissipated energies share the same stress response and have different strain rates, implying that the ratio of two dissipated energy rates ($E_{solid/fluid}$) represents a comparison between acquisitions from recoverable and unrecoverable components.

Using this definition, we observe that at small amplitudes, when the recoverable component is dominant, $E_{solid/fluid} > 1$, while at large amplitude, when most of the material's response is unrecoverable, $E_{solid/fluid} < 1$.

We show in Fig. 13 the energetic Deborah number, $E_{solid/fluid}$, for the GO suspension and gel during the oscillation cycle (see the supplementary material Fig. S7 for each dissipated energy ratio). The two GO colloids show similar behaviors at small and large amplitudes but exhibit different behavior at intermediate amplitudes, as in the case of the traditional amplitude sweep metrics. As the amplitude increases, the $E_{solid/fluid}$ decreases and becomes less than 1 at intermediate amplitude as marked by the green area in Fig. 13. The GO suspension exhibits a gradual decrease in the $E_{solid/fluid}$, while GO gel remains around 1 at intermediate amplitude and then decreases almost discontinuously.

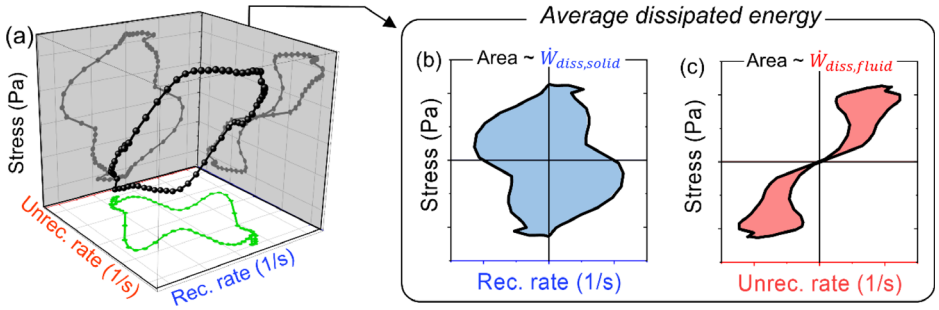

FIG. 12. (a) The same 3D Lissajous curve as in Fig. 9(a). The stress plotted as a function of (b) recoverable rate and (c) unrecoverable rate. The blue/red area is proportional to the solid/fluid dissipated energy.

We attribute this difference in $E_{solid/fluid}$ to the microstructures of the GO suspension and gel. As discussed in association with Figs. 4 and 10, the GO gel shows local yielding behavior due to the Ca^{2+}, while the yielding behavior of the GO suspension comes from the rearrangement of the GO sheets.

The energetic description via strain decomposition allows us to replace the ratio of two dissipated energy rates with the Deborah number of yield stress fluid during the oscillation cycle. The $E_{solid/fluid}$ is a dimensionless number that describes which rate of energy dissipation is dominant on average during an oscillation cycle. At any amplitude, a material may yield either completely or incompletely, and contributions of the recoverable and unrecoverable components are always present, but the contribution varies quantitatively with amplitudes. Thus, the trend of the $E_{solid/fluid}$ with increasing amplitude can explain how the GO suspension gel yields: a continuous transition from the recoverable and unrecoverable acquisition of strain.

IV. SUMMARY AND CONCLUSION

This study investigates the yielding behavior of a graphene oxide (GO) suspension and gel using recovery rheology. While traditional rheology interprets the loss modulus, G″, as a viscous property that represents liquid-like behavior, recovery rheology shows that G″ is composite and can be decomposed into components that relate to the rates at which strain is acquired recoverably and unrecoverably. Based on the decomposition of strain and moduli, recovery rheology provides more information about the material's deformation as recoverable (viscoelastic solid) and unrecoverable (plastic) responses. From the results, the contribution of recovery rheology to understanding yielding behavior can be summarized as follows:

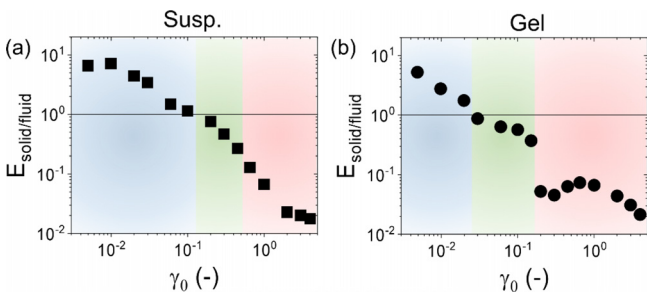

FIG. 13. The ratio of two dissipated energy rates ($E_{solid/fluid}$) for (a) GO suspension and (b) gel.

1. *Decomposition of G″ and LAOS type.* In a traditional amplitude sweep, the GO suspension is classified as type-I (no overshoot in dynamic moduli), while the GO gel is classified as type-III (overshoot in G″ only). However, once recovery rheology decomposes G″ into recoverable (G''_{solid}) and unrecoverable (G''_{fluid}) components, in Fig. 4, the GO suspension is shown to have an overshoot in G''_{fluid}, while the gel has overshoots in both G''_{solid} and G''_{fluid}. These observations indicate an increased contribution of the plastic component to dissipated energy. Yielding may therefore always be associated with an overshoot in G''_{fluid}, regardless of whether the traditional loss modulus overshoots or not. Our results, which include the decomposed moduli, also suggest that the LAOS type, which was previously determined based on G′ and G″ alone, can be further subdivided according to the decomposed moduli in the supplementary material (Fig. S3).
2. *The physical meaning of G′-G″ intersection.* The amplitude dependence of the recoverable and unrecoverable contributions has shown a clear physical meaning of the G′-G″ intersection, which some have referred to as the yield point, while others have called the flow point. The amplitude at which the moduli cross is the maximum amount of recoverable strain acquirable by the system. In Fig. 5, the recoverable strain does not exceed beyond the amplitude of G′-G″ crossover.
3. *Guidelines for energy efficiency.* As a result, the energy stored elastically levels off, while the amount of energy dissipated keeps increasing with a further increase in the amplitude over the G′-G″ intersection. The amount of energy that can be recovered is therefore finite, and at high shear forces, only the dissipated energy increases. This means that larger shear forces result in lower energetic efficiency of the processing and also that the application of large forces does not completely fluidize the system. Even at the highest rates and largest forces, we continued to measure significant recoverable strain, indicating that if the goal is to erase previous flow memories, one needs to also remove the recoverable strain.[63,64] Hence, a high shear force is not always ideal for the extrusion of inks, because it reduces the energy efficiency of the printing. It is energetically favorable, though not always fastest, to apply the lowest shear force at which the ink extrusion begins to reduce the processing energy waste.
4. *Yielding as a continuous energy transition.* The decomposed strain provides three energetic descriptions of energy stored from viscoelastic solid and energy dissipated from viscoelastic solid and plastic properties. From small to large amplitude, all three energetic contributions are always present, but their contributions depend on amplitude. This indicates that (1) energy is

being stored elastically even when the material flows at large amplitudes and (2) the material yields via a continuous transition from viscoelastic solid to plastic contribution as shown in Sec. III D. Interpreting that "materials flow after the yield point" is an oversimplification.

5. *Energetic Deborah number ($E_{solid/fluid}$).* Beyond the oversimplification of the yield point, we propose and show the utility of a dimensionless number that quantifies the material's deformation as solid-like and fluid-like by comparing the time-averaged energies acquired from recoverable and unrecoverable rates during the oscillation. The ratio of two dissipated energy rates ($E_{solid/fluid}$), in Fig. 13 can quantitatively describe the deformation of the GO suspension and gel as solid-like and fluid-like deformations, and its interpretation is equivalent to that of the Deborah number. The GO suspension exhibits a gradual decrease in $E_{solid/fluid}$, indicating the gradual rearrangement of the GO sheets, whereas the GO gel shows that $E_{solid/fluid}$ stays around 1 at intermediate amplitudes and then steeply decreases at large amplitudes, implying that yielding occurs as the agglomerates break.

The GO suspension and gel used in this study have similar G′ and G″, and there is no significant difference in their linear behaviors. However, two GO colloids have different limits of the stored energy, which is related to the phenomenon of mechanical memory, and yield through different pathways. These findings provide more abundant information that the current approaches for the ink characterization focusing on the linear viscoelastic properties. This study emphasizes that effective guidelines for DIW printing can be established through a clear understanding of how materials yield. Furthermore, the way to understand yielding behavior through recovery rheology proposed in this study can be applied to various yield stress fluids, not only GO colloids, and thus can be used generally for processes involving yielding such as extrusion, squeeze, and spread.

SUPPLEMENTARY MATERIAL

See the supplementary material for the following details: amplitude sweep results for various GO concentrations in the suspension and gel series samples; schematic illustration of the GO suspension and gel; decomposition of the LAOS type; stored energy as a function of amplitude; traditional Lissajous curve; correlation between $G''_{fluid,raw}$ and the steady-shear viscosity (η_{flow}); and dissipated energy ratio as a function of amplitude.

ACKNOWLEDGMENTS

This research was supported by the Basic Science Research Program through the National Research Foundation of Korea (NRF) funded by the Ministry of Education (No. NRF-2021R1A6A3A03039172). This material was based upon work supported by NSF Grant No. 1847389.

AUTHOR DECLARATIONS

Conflict of Interest

The authors have no conflicts to disclose.

Author Contributions

Yul Hui Shim: conceptualization (equal); formal analysis (lead); funding acquisition (equal); writing—original draft (lead); and writing—review and editing (equal). **Simon Rogers:** conceptualization (equal); funding acquisition (equal); and writing—review and editing (equal).

DATA AVAILABILITY

The data that support the findings of this study are available from the corresponding author upon reasonable request.

REFERENCES

[1]J. E. Kim, T. H. Han, S. H. Lee, J. Y. Kim, C. W. Ahn, J. M. Yun, and S. O. Kim, "Graphene oxide liquid crystals," Angew. Chem. Int. Ed. **50**, 3043 (2011).
[2]Z. Xu and C. Gao, "Aqueous liquid crystals of graphene oxide," ACS Nano **5**, 2908 (2011).
[3]P. Kumar, U. N. Maiti, K. E. Lee, and S. O. Kim, "Rheological properties of graphene oxide liquid crystal," Carbon **80**, 453 (2014).
[4]S. Naficy, R. Jalili, S. H. Aboutalebi, R. A. Gorkin III, K. Konstantinov, P. C. Innis, G. M. Spinks, P. Poulin, and G. G. Wallace, "Graphene oxide dispersions: Tuning rheology to enable fabrication," Mater. Horiz. **1**, 326 (2014).
[5]J. K. Wychowaniec, M. Iliut, B. Borek, C. Muryn, O. O. Mykhaylyk, S. Edmondson, and A. Vijayaraghavan, "Elastic flow instabilities and macroscopic textures in graphene oxide lyotropic liquid crystals," npj 2D Mater. Appl. **5**, 11 (2021).
[6]A. Ojha, H. Ibrahim, N. Alyabyeva, R. Lazzari, M. Goldmann, and P. Thareja, "Nanosheet size-dependent rheology, microstructure, adsorption properties of graphene oxide-electrolyte dispersions and adsorbents," Synth. Met. **269**, 116494 (2020).
[7]C. Valles, R. J. Young, D. J. Lomax, and I. A. Kinloch, "The rheological behavior of concentrated dispersions of graphene oxide," J. Mater. Sci. **49**, 6311 (2014).
[8]Y. H. Shim, K. E. Lee, T. J. Shin, S. O. Kim, and S. Y. Kim, "Wide concentration liquid crystallinity of graphene oxide aqueous suspension with interacting polymers," Mater. Horiz. **4**, 1157 (2017).
[9]Y. Jiang, Z. Xu, T. Huang, Y. Liu, F. Guo, J. Xi, W. Gao, and C. Gao, "Direct 3D printing of ultralight graphene oxide aerogel microlattices," Adv. Funct. Mater. **28**, 1707024 (2018).
[10]H. Bai, C. Li, X. Wang, and G. Shi, "On the gelation of graphene oxide," J. Phys. Chem. C **115**, 5545 (2011).
[11]Y. H. Shim, K. E. Lee, T. J. Shin, S. O. Kim, and S. Y. Kim, "Tailored colloidal stability and rheological properties of graphene oxide liquid crystals with polymer-induced depletion attractions," ACS Nano **12**, 11399 (2018).
[12]Y. Shao, H. Wang, Q. Zhang, and Y. Li, "Fabrication of large-area and high-crystallinity photoreduced graphene oxide films via reconstructed two-dimensional multilayer structures," NPG Asia Mater. **6**, e119 (2014).
[13]J. H. Kim, Y. Choi, J. Kang, E. Choi, S. E. Choi, O. Kwon, and D. W. Kim, "Scalable fabrication of deoxygenated graphene oxide nanofitration membrane by continuous slot-die coating," J. Membr. Sci. **612**, 118454 (2020).
[14]A. Akbari, P. Sheath, S. T. Martin, D. B. Shinde, M. Shaibani, P. C. Banerjee, R. Tkacz, D. Bhattacharyya, and M. Majumder, "Large-area graphene-based nanofiltration membranes by shear alignment of discotic nematic liquid crystals of graphene oxide," Nat. Commun. **7**, 10891 (2016).
[15]W. Eom, H. Shin, R. B. Ambade, S. H. Lee, K. H. Lee, D. J. Kang, and T. H. Han, "Large-scale wet-spinning of highly electroconductive MXene fibers," Nat. Commun. **11**, 2825 (2020).
[16]H. Park, K. H. Lee, Y. B. Kim, S. B. Ambade, S. H. Noh, W. Eom, J. Y. Hwang, W. J. lee, J. Huang, and T. H. Han, "Dynamics assembly of liquid crystalline graphene oxide gel fibers for ion transport," Sci. Adv. **4**, eaau2104 (2018).
[17]G. Xin, W. Zhu, Y. Deng, J. Cheng, L. T. Zhang, A. J. Chung, S. De, and J. Lian, "Microfluidics-enabled orientation and microstructure control of macroscopic graphene fibres," Nat. Nanotechnol. **14**, 168 (2019).
[18]Y. H. Shim, H. Ahn, S. Lee, S. O. Kim, and S. Y. Kim, "Universal alignment of graphene oxide in suspensions and fibres," ACS Nano **15**, 13453 (2021).

[19]J. Zhong, G. X. Zhou, P. G. He, Z. H. Yang, and D. C. Jia, "3D printing strong and conductive geo-polymer nanocomposite structures modified by graphene oxide," Carbon **117**, 421 (2017).
[20]W. Cao, S. Ling, H. Chen, H. He, X. Li, and C. Zhang, "3D-printed ultralight, superelastic reduced graphene oxide/manganese dioxide foam for high-performance compressible supercapacitors," Ind. Eng. Chem. Res. **61**, 10922 (2022).
[21]A. Corker, H. C. Ng, R. J. Poole, and E. Garcia-Tunon, "3D printing with 2D colloids: Designing rheology protocols to predict 'printability' of soft-materials," Soft Matter **15**, 1444 (2019).
[22]S. Tagliaferri, A. Panagiotopoulos, and C. Mattevi, "Direct ink writing of energy materials," Mater. Adv. **2**, 540 (2021).
[23]M. A. S. R. Saadi, A. Maguire, N. T. Pottackal, M. S. H. Thakur, M. M. Ikram, A. J. Hart, P. M. Ajayan, and M. M. Rahman, "Direct ink writing: A 3D printing technology for diverse materials," Adv. Mater. **34**, 2108855 (2022).
[24]E. Garcia-Tunon, R. Agrawal, B. Ling, and D. J. C. Dennis, "Fourier-transform rheology and printability maps of complex fluids for three-dimensional printing," Phys. Fluids **35**, 017113 (2023).
[25]A. Das, J. A. Riet, M. J. Bortner, and C. Mcllroy, "Rheology, crystallization, and process conditions: The effect on interlayer properties in three-dimensional printing," Phys. Fluids **34**, 123108 (2022).
[26]E. Pulatsu and C. Udenigwe, "Perspectives, analyses, and progress in additive manufacturing of food," Phys. Fluids **35**, 031303 (2023).
[27]A. M'Barki, L. Bocquet, and A. Stevenson, "Linking rheology and printability for dense and strong ceramics by direct ink writing," Sci. Rep. **7**, 6017 (2017).
[28]C. E. Cipriani, Y. Shu, E. B. Pentzer, and C. C. Benjamin, "Viscoelastic and thixotropic characterization of paraffin/photopolymer composites for extrusion-based printing," Phys. Fluids **34**, 093106 (2022).
[29]S. S. L. Chan, R. M. Pennings, L. Edwards, and G. V. Franks, "3D printing of clay for decorative architectural applications: Effect of solids volume fraction on rheology and printability," Addit. Manuf. **35**, 101335 (2020).
[30]M. Monteferrante, A. Montessori, S. Succi, D. Pisignano, and M. Lauricella, "Lattice Bolzmann multicomponent model for direct-writing printing," Phys. Fluids **33**, 042103 (2021).
[31]E. Erfanian, R. Moaref, R. Ajdary, K. C. Tam, O. J. Rojas, M. Kamkar, and U. Sundararaj, "Electochemically synthesized graphene/TEMPO-oxidized cellulose nanofibrils hydrogels: Highly conductive green inks for 3D printing of robust structured EMI shielding aerogels," Carbon **210**, 118037 (2023).
[32]S. M. A. Ojagh, M. Amini, C. Cranmer-Smith, F. Vahabzadeh, K. C. Tam, O. J. Rojas, M. Kamkar, and T. G. M. van de Ven, "Crystalline and hairy nanocelluloses for 3D printed hydrogels and strongly structured cryogels," ACS Sustainable Chem. Eng. **11**, 5674 (2023).
[33]A. Ghaffarkhah, M. Kamkar, Z. A. Dijvejin, H. Riazi, S. Ghaderi, K. Golovin, M. Soroush, and M. Arjmand, "High-resolution extrusion printing of Ti_3C_2-based inks for wearable human motion monitoring and electromagnetic interference shielding," Carbon **191**, 277 (2022).
[34]K. E. Haddad, C. Aumnate, C. Saengow, M. A. Kanso, S. J. Coombs, and A. J. Giacomin, "Complex viscosity of graphene suspensions," Phys. Fluids **33**, 093109 (2021).
[35]Y. Kim, S. Kim, B. S. Kim, J. H. Park, K. H. Ahn, and J. D. Park, "Yielding behavior of concentrated lithium-ion battery anode slurry," Phys. Fluids **34**, 123112 (2022).
[36]Y. Wei, R. Li, and H. Zhang, "Measures of the yield stress fluids oriented for dysphagia management using steady-state shear, transient shear, and large-amplitude oscillatory shear (LAOS)," Phys. Fluids **34**, 123107 (2022).
[37]H. Ji, J. Zhao, J. Chen, S. Shimai, J. Zhang, Y. Liu, D. Liu, and S. Wang, "A novel experimental approach to quantitatively evaluate the printability of inks in 3D printing using two criteria," Addit. Manuf. **55**, 102846 (2022).
[38]J. L. Dávila and M. A. d'Ávila, "Rheological evolution of Laponite/alginate inks for 3D extrusion-based printing," Int. J. Adv. Manuf. Technol. **101**, 675 (2019).
[39]V. Kokol, Y. B. Pottathara, M. Mihelčič, and L. S. Perše, "Rheological properties of gelatin hydrogels affected by flow- and horizontally-induced cooling rates during 3D cryo-printing," Colloids Surf. A **616**, 126356 (2021).
[40]F. Afghah, M. Altunbek, C. Dikyol, and B. Koc, "Preparation and characterization of nanoclay-hydrogel composite support-bath for bioprinting of complex structures," Sci. Rep. **10**, 5257 (2020).
[41]J. C.-W. Lee, K. M. Weigandt, E. G. Kelley, and S. A. Rogers, "Structure-property relationships via recovery rheology in viscoelastic materials," Phys. Rev. Lett. **122**, 248003 (2019).
[42]G. J. Donley, P. K. Singh, A. Shetty, and S. A. Rogers, "Elucidating the G″ overshoot in soft materials with a yield transition via a time-resolved experimental strain decomposition," Proc. Natl. Acad. Sci. U. S. A. **117**, 21945 (2020).
[43]K. Kamani, G. J. Donley, and S. A. Rogers, "Unification of the rheological physics of yield stress fluids," Phys. Rev. Lett. **126**, 218002 (2021).
[44]J. J. Griebler and S. A. Rogers, "The nonlinear rheology of complex yield stress foods," Phys. Fluids **34**, 023107 (2022).
[45]K. Weissenberg, "A continuum theory of rheological phenomena," Nature **159**, 310 (1947).
[46]M. Reiner, "Rheology," in *Elasticity and Plasticity/Elastizität Und Plastizität, Encyclopedia of Physics/Handbuch Der Physik*, edited by S. Flügge (Springer, Berlin/Heidelberg, 1958), pp. 434–550.
[47]K. Hyun, S. H. Kim, K. H. Ahn, and S. J. Lee, "Large amplitude oscillatory shear as a way to classify the complex fluids," J. Non-Newtonian Fluid Mech. **107**, 51 (2002).
[48]S. Park, K. Lee, G. Bozoklu, W. Cai, S. T. Nguyen, and R. S. Ruoff, "Graphene oxide papers modified by divalent ions-enhancing mechanical properties via chemical cross-linking," ACS Nano **2**, 572–578 (2008).
[49]J. L. Suter and P. V. Coveney, "Principles governing control of aggregation and dispersion of aqueous graphene oxide," Sci. Rep. **11**, 22460 (2021).
[50]W. Eom, H. Park, S. H. Noh, K. H. Koh, K. Lee, W. J. Lee, and T. H. Han, "Strengthening and stiffening graphene oxide fibers with trivalent metal ion binders," Part. Part. Syst. Charact. **34**, 1600401 (2017).
[51]N. W. Tschoegl, *The Phenomenological Theory of Linear Viscoelastic Behavior* (Springer, Berlin Heidelberg, 1989).
[52]J. D. Ferry, *Viscoelastic Properties of Polymer Solutions* (Wiley, New York, 1980).
[53]Y. H. Shim and S. Y. Kim, "Continuous structural deformation of graphene oxide liquid crystal colloids under shear for hydrogel films," Carbon **202**, 358 (2023).
[54]G. M. Choi, M. Park, S. Y. Jeong, and H. S. Lee, "Orientation effect on the rheology of graphene oxide dispersions in isotropic phase, ordered isotropic biphase, and discotic phase," J. Rheol. **65**, 791 (2021).
[55]C. Zhao, P. Zhang, J. Zhou, S. Qi, Y. Yamauchi, R. Shi, R. Fang, Y. Ishida, S. Wang, A. P. Tomsia, M. Liu, and L. Jiang, "Layered nanocomposites by shear-flow-induced alignment of nanosheets," Nature **580**, 210 (2020).
[56]J. G. Oldroyd, "Rectilinear plastic flow of a Bingham solid—III: A more general discussion of steady flow," Math. Proc. Cambridge Philos. Soc. **44**, 200 (1948).
[57]P. Coussot and S. A. Rogers, "Oldroyd's model and the foundation of modern rheology of yield stress fluids," J. Non-Newtonian Fluid Mech. **295**, 104604 (2021).
[58]S. A. Rogers, B. M. Erwin, and D. Vlassopoulos, "A sequence of physical processes determined and quantified in LAOS: Application to a yield stress fluid," J. Rheol. **55**, 435 (2011).
[59]K. Kamani, G. J. Donley, R. Rao, A. M. Grillet, C. Roberts, A. Shetty, and S. A. Rogers, "Understanding the transient large amplitude oscillatory shear behavior of yield stress fluids," J. Rheol. **67**, 331 (2023).
[60]M. Reiner, "The Deborah number," Phys. Today **17**(1), 62 (1964).
[61]R. Poole, "The Deborah number and Weissenberg numbers," Br. Soc. Rheol., Rheol. Bull. **53**(2), 32 (2012).
[62]P. K. Singh, J. C.-W. Lee, K. A. Patankar, and S. A. Rogers, "Revisiting the basis of transient rheological material functions: Insights from recoverable strain measurements," J. Rheol. **65**, 129 (2021).
[63]J. Choi and S. A. Rogers, "Optimal conditions for pre-shearing thixotropic or aging soft materials," Rheol. Acta **59**, 921 (2020).
[64]S. Jamali and G. H. McKinley, "The Mnemosyne number and the rheology of remembrance," J. Rheol. **66**, 1027 (2022).